INTERSTELLAR HELIUM IN INTERPLANETARY SPACE

William C. Feldman, J. J. Lange, and F. Scherb

ABSTRACT The velocity distribution function of He^+ in the solar wind at 1 AU is calculated with the assumption that the source is photoionization of a cold ($T = 100°$ K), neutral interstellar wind. If the spiral magnetic field is noise free, the velocity distribution is diffuse and would not produce a peak at $4(E/Q)_H$ in an E/Q particle spectrum. If the velocity of the interstellar wind with respect to the sun lies in the ecliptic, a large variation of the He^+ number density with respect to ecliptic longitude is expected.

INTRODUCTION

A peak appearing at four times the energy/charge (E/Q) location of the hydrogen peak in two Vela 3 electrostatic analyzer spectra of solar wind ions was interpreted as being mostly due to He^+ [*Bame et al.*, 1968]. The He^+ abundance relative to He^{++} was measured to be $3\times10^{-3}\pm50$ percent (Bame, p.548). Two other spectra published by *Bame et al.* [1968] yielded only an upper limit of 10^{-3} for $n_{He^+}(r_e)/n_{He^{++}}(r_e)$, the ratio of number densities at $r = r_e = 1$ AU. A more recent attempt [*Bame et al.*, 1970] to determine the mass and charge composition in the solar wind attributed a peak located at four times the E/Q location of H^+ as probably due to Si^{7+} instead of He^+.

The Vela 3 observation cannot be explained simply since $n_{He^+}(r_e)/n_{He^{++}}(r_e)$ is expected to be of the order of 3×10^{-6} for a 10^6 °K corona [*Tucker and Gould*, 1966]. *Hundhausen et al.* [1968] attempted an explanation in terms of a model proposed earlier by *Patterson et al.* [1963]. This model considers the solar wind protons converted by charge exchange with galactic hydrogen into hot, isotropic neutral hydrogen atoms at an assumed spherical shock boundary surrounding the heliosphere. These fast neutrals flow in toward the sun where a small fraction charge exchange with the solar wind He^{++} to produce the He^+. They find that if 1 percent of the solar wind protons find their way back and interact within 1 AU, enough He^+ could be produced to explain the Vela 3 data. *Holzer and Axford* [1970] tried to explain the ratio of 3×10^{-3} by assuming that the solar system is moving through an interstellar gas cloud. Neutral He would be gravitationally focused by the sun, photoionized, and then incorporated into the solar wind as He^+.

Rocket observations of diffuse extreme ultraviolet radiation (EUV) [*Young et al.*, 1968, *Johnson et al.*, 1971*a*] from the night sky yielded an upper limit of 2 R of 584Å radiation [*Johnson et al.*, 1971*b*]. If all diffuse 584Å radiation were to be interpreted as due to the solar 584Å line backscattered by neutral He in interplanetary space, then 2 R corresponds to $n_{He}(\infty) \simeq 3\times10^{-2}$ cm^{-3}. This is not a restriction to the *Holzer and Axford* [1970] interpretation of the Vela 3 measurements.

In this paper we consider the orbits of interstellar He^+ ions injected into an ideal (noise-free) Archimedean spiral magnetic field. The He^+ ions originate from infalling interstellar wind neutral He atoms that are ionized in the interplanetary medium. We thus determine the velocity distribution function of He^+ expected at 1 AU as a function of azimuthal position ϕ in the ecliptic for different interstellar wind parameters. This study also gives orbits of atoms or molecules that escape from solar system bodies and are ionized in interplanetary space. An example of such a source could be neutral hydrogen ionized beyond the disturbed interface between the Venusian ionosphere and the solar wind. Detection and identification of such particles could yield information concerning atmospheric abundances and thermalization processes in the solar wind. Finally, we

W. C. Feldman, Los Alamos Scientific Laboratory, Los Alamos, New Mexico; J. J. Lange, Wright Patterson Air Force Base, Ohio; F. Scherb, University of Wisconsin, Madison, Wisconsin.

compare the various interpretations of infalling neutral He within the interplanetary medium.

PITCH ANGLE SCATTERING BY MAGNETIC IRREGULARITIES IN THE SOLAR WIND

Before proceeding to a discussion of the orbits of very low-energy charged particles injected into the solar wind, we consider the magnitude of the perturbation caused by cyclotron-resonant pitch-angle scattering from magnetic irregularities convected by the solar wind. The problem with relevance to the low-energy particles of interest here has been treated theoretically by *Sturrock* [1966] and *Hall and Sturrock* [1967], and applied by *Barnes* [1970] to fast particles accelerated at the earth's bow shock and moving upstream in the solar wind. Assuming the dominant scattering process is pure magnetic cyclotron-resonant pitch-angle scattering, the particle velocity pitch-angle distribution function F is well approximated by a diffusion equation of the form

$$\frac{DF}{Dt} = \left(\frac{\partial}{\partial t} + V_{\|}\frac{\partial}{\partial Z}\right)F \cong \frac{1}{\sin\theta}\frac{\partial}{\partial\theta}\left[\sin\theta G(V_{\|})\frac{\partial F}{\partial\theta}\right]$$

where $V_{\|}$ is the particle's velocity component parallel to the unperturbed magnetic field B_O, and

$$G(V_{\|}) = \frac{\pi^2\nu^2}{B_O{}^2}\,P(\nu')$$

where $\nu = eB_O/2\pi mc$ is the cyclotron frequency, and $P(\nu')$ is the power density spectrum of the transverse magnetic field fluctuations evaluated at the frequency ν', which is Doppler shifted into the cyclotron frequency in the rest frame of the particle. To obtain an order of magnitude of the time scale τ for the disruption of a beam of He^+ particles moving relative to the solar wind, we approximate G as a constant and set $x = \cos\theta$ so that

$$\frac{DF}{Dt} = G\frac{d}{dx}\left[(1-x^2)\frac{dF}{dx}\right]$$

In the frame of reference moving with the particle beam

$$F(x,t) = \sum_{l=0}^{\infty}\exp\left[-l\,(l+1)Gt\,P_l(x)\right]$$

where the $P_l(x)$ are lth-order Legendre polynomials. Thus the decay time τ_l is given by

$$\tau_l = \frac{1}{l(l+1)G}$$

Power spectra of the interplanetary magnetic field have been reported by *Coleman* [1966] for the Mariner 2 magnetometer, by *Siscoe et al.* [1968] for the Mariner 4 magnetometer, and by *Sari and Ness* [1969] for the Pioneer 6 magnetometer. Comparison of these results indicates that the power level at a given frequency can vary significantly depending on solar activity. Since the He^+ particles to be discussed later are for the most part moving away from the sun, a conservative choice of frequency for evaluating the power spectrum is the cyclotron frequency which for He^+ in a 6γ magnetic field (at 1 AU) is 2.3×10^{-2} Hz. Choosing $P(2\times10^{-2}\text{ Hz}) = 3\times10^{-1}\gamma^2/\text{Hz}$ from Mariner 4 data for quiet periods yields

$$2G = 2\times10^{-6}\text{ sec}^{-1}$$

and consequently $\tau_1 = 5\times10^5$ sec. But 5×10^5 sec is about equal to the expected ion transit times from $r = 0.1$ AU to 1 AU if the He radial velocity at the point of ionization is away from the sun.

This estimate for τ is probably uncertain by at least two orders of magnitude due primarily to the approximate nature of the diffusion equation, the evaluation of P at 1 AU and the choice of $l = 1$. Of course, more peaked pitch-angle distribution functions are characterized by higher l values and so are damped more quickly. Most important, because it is unknown experimentally, is the radial dependence of the power spectrum evaluated at the Doppler shifted gyrofrequency. Evidence from Mariner 4 magnetic field data [*Coleman et al.*, 1969] indicates that the power density for a given frequency generally decreases roughly as r^{-2} for 1 AU $< r <$ 1.43 AU where r is the heliocentric distance. but as r increases, B decreases and so does the gyrofrequency. The radial dependence relevant to our problem is that of the power density spectrum evaluated at the Doppler shifted gyrofrequency. From figure 14 of *Coleman et al.* [1969] it is seen that this is almost independent of r for 1 AU $< r <$ 1.43 AU. In any case, it is expected to be less dependent upon r than the power density spectrum evaluated at a fixed frequency.

Considering these uncertainties coupled with the measured variability of the solar wind, one can conclude neither that significant pitch-angle scattering occurs in transit to 1 AU nor that the He^+ orbits remain unperturbed by magnetic field fluctuations. Furthermore, as pointed out by *Barnes* [1970], τ_1 refers only to the disruption of the beam by hydromagnetic waves but not to thermalization. The time scale for thermalization is expected to be longer.

It is thus useful to determine the unperturbed orbits in an ideal spiral magnetic field as a function of injection

position and velocity. It is expected that particles injected at small r will undergo some degree of pitch-angle scattering, whereas those injected around 1 AU will follow unperturbed orbits. One can then compare future measurements of the He^+ velocity distribution function with both the thermalized and unperturbed limits to obtain information concerning interstellar wind parameters as well as wave-particle interactions in the solar wind.

UNPERTURBED ORBITS OF A TEST PARTICLE INJECTED INTO THE SOLAR WIND

The coordinate system relevant to this discussion is shown in figure 1. The sun is assumed to move with velocity $\langle V_\infty \rangle$ relative to a cold ($T = 100^\circ$ K) interstellar cloud such that in the frame of reference with the sun at rest at the origin, neutral He atoms appear to be moving parallel to the YZ plane at an angle Θ with respect to the Z axis. The positive Z axis is oriented northward perpendicular to the ecliptic. The XY plane is coincident with the ecliptic. Infalling He atoms follow hyperbolic trajectories before being ionized by solar EUV. After ionization they are accelerated by a radially convected spiral magnetic field. Although the spiral magnetic field pattern is cylindrically symmetric, the subsequent charged particle trajectories are not, due to the asymmetric initial injection velocities.

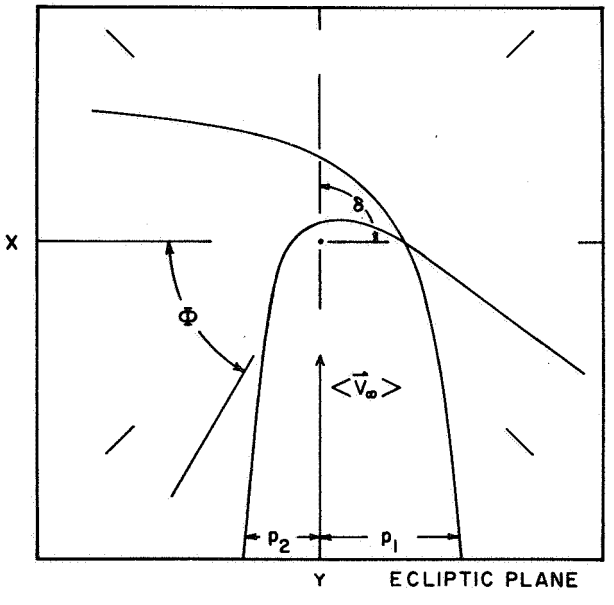

Figure 1 *Interstellar infall coordinate system with* $\langle V_\infty \rangle$ *in the ecliptic.*

Each He atom hyperbolic orbit is planar. Every point in the orbit plane can be specified equivalently by r, the radial distance from the sun, and δ, the angle between $\mathbf{r}$ and $\langle V_\infty \rangle$, or by two impact parameters p_1 and p_2 identifying both a direct and indirect orbit, respectively, which pass through that point. *Fahr* [1968] obtained an expression for the neutral number density $n^0_{He}(\mathbf{r})$ at any point for $T = 0^\circ$ K using the continuity equation. Rewriting his results we obtain

$$n^0_{He}(\mathbf{r}) = n_1 \exp\left[\frac{-r_e^2 P(r_e)(\pi - \delta)}{\langle V_\infty \rangle p_1}\right] + n_2 \exp\left[\frac{-r_e^2 P(r_e)(\pi + \delta)}{\langle V_\infty \rangle p_2}\right] \qquad (1)$$

where

$$n_1 = \left(\frac{p_1^2}{p_1^2 - p_2^2}\right) n_{He}(\infty)$$

$$n_2 = n_1 - n_{He}(\infty)$$

$$p_1 = \frac{r \sin\delta}{2} + \left[\left(\frac{r \sin\delta}{2}\right)^2 + rb(1 + \cos\delta)\right]^{1/2}$$

$$p_2 = p_1 - r \sin\delta$$

$$b = \frac{GM}{\langle V_\infty \rangle^2}$$

and $n_{He}(\infty)$ is the number density of neutral He at $r = \infty$, $P(r_e)$ is the probability per sec for ionization at $r_e = 1$ AU, G is the gravitational constant, and M is the solar mass; $P(r_e)$ is variable, but is chosen here as

$$P(r_e) = 6.8 \times 10^{-8} \text{ sec}^{-1}$$

In figures 2 and 3, we plot two cuts through the normalized neutral He number density distribution $n^0_{He}(r)/n_{He}(\infty)$. The radial dependence of $n^0_{He}(r)/n_{He}(\infty)$ for $\langle V_\infty \rangle = 20$ km/sec oriented in the ecliptic ($\Theta = 90^\circ$) is plotted in figure 2 for ecliptic positions oriented at right angles to $\langle V_\infty \rangle$. One sees that, beyond 1 AU, $n^0_{He}(r)/n_{He}(\infty)$ is essentially constant. On the other hand, the azimuthal dependence is dominated by a dense tail in the antiapex direction. This feature is characteristic of the gravitational focusing problem; it is real and limited only by the temperature of the infalling

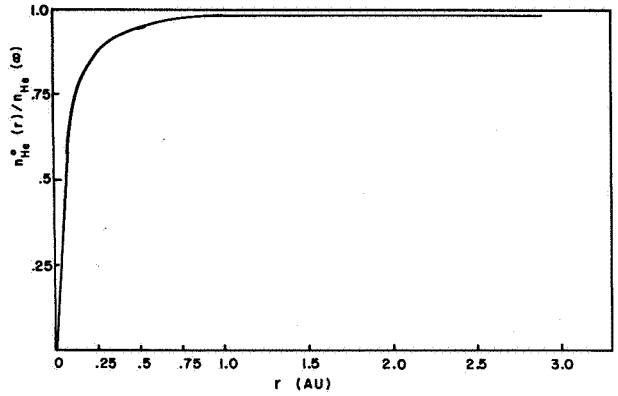

Figure 2 *Normalized neutral* He *number density as a function of heliocentric distance:* $\langle V_\infty \rangle = 20$ *km/sec,* $\Theta = 90°$, $\phi = 0°$ *or* $180°$.

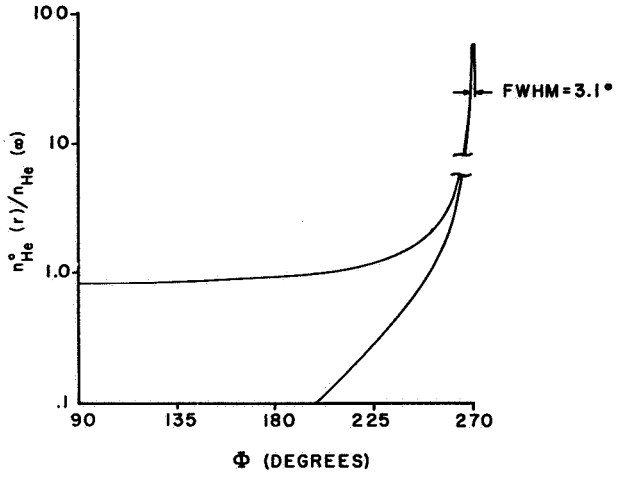

Figure 3 *Normalized neutral* He *number density as a function of azimuth:* $\langle V_\infty \rangle = 20$ *km/sec,* $T = 100°$K, $r = 0.5$ *AU. The* He *density plotted in the neighborhood of* $\phi = 270°$ *is the sum of contributions from both direct and indirect orbits.*

gas. For $\delta = 0$ and $T = 0°$ K, $p_1 = p_2$; hence, both n_1 and $n_2 = \infty$. For T different from zero but such that $m\langle V_\infty \rangle^2 / 2kT \gg 1$, we can obtain an analytic expression for n_1 and n_2 at $\delta = 0$ by integrating $n^0_{\mathrm{He}}(r)$ weighted by an isotropic maxwellian velocity distribution function over V_∞. The velocity-space coordinate system for this calculation is outlined in figure 4.

For $\delta \ll 1$, we can write a maxwellian distribution in the form

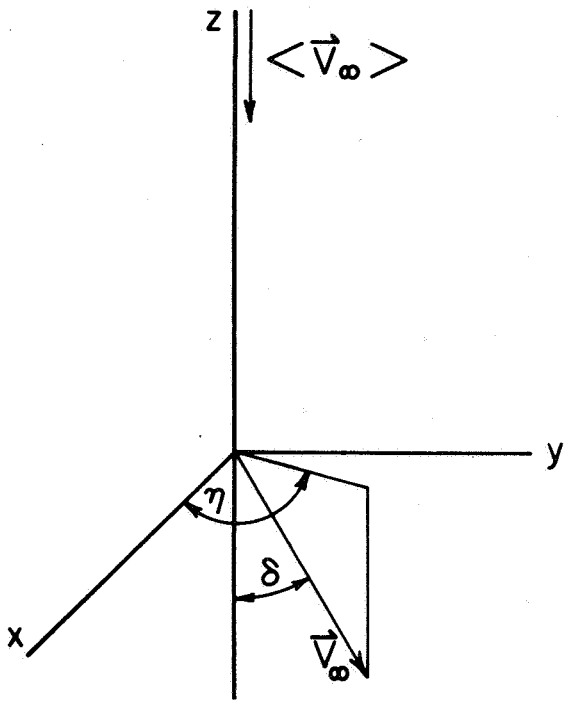

Figure 4 *Velocity space coordinate system relevant to calculation of the neutral* He *number density for* $\delta = 0$.

$$F(V_\infty) d^3 V_\infty = \left(\frac{m}{2\pi kT}\right)^{3/2} \exp\left[\frac{-m(V_\infty - \langle V_\infty \rangle)^2}{2kT}\right]$$

$$\exp\left[\frac{-mV_\infty \langle V_\infty \rangle \delta^2}{2kT}\right] d^3 V_\infty$$

Then,

$$n_{\mathrm{He}}(r, o) =$$

$$\int_0^\infty \int_0^\pi \int_0^{2\pi} n^0_{\mathrm{He}}(r,o) F(V_\infty) V_\infty^2 \, dV_\infty \sin\delta \, d\delta \, d\eta$$

To find $n^0_{\mathrm{He}}(r, \delta)$, note that

$$\lim_{\delta \to 0} p_1 = (2br)^{1/2} \qquad \lim_{\delta \to 0} (p_1 - p_2) = r\delta$$

hence

$$n^0_{\mathrm{He}}(r,\delta) = \frac{1}{\delta} n_{\mathrm{He}}(\infty) \left(\frac{2b}{r}\right)^{1/2} \exp\left[\frac{-\pi r_e^2 P(r_e)}{(2br)^{1/2} \langle V_\infty \rangle}\right]$$

and

$$n_{\mathrm{He}}(r,o)$$

$$= 2\pi n_{\mathrm{He}}(\infty)\left(\frac{m}{2\pi kT}\right)^{3/2}\left(\frac{2b}{r}\right)^{1/2}\exp\left[\frac{-\pi r_e^2 P(r_e)}{(2br)^{1/2}\langle V_\infty\rangle}\right]\times$$

$$\int_0^\infty \frac{\langle V_\infty\rangle}{V_\infty}\exp\left[\frac{(V_\infty-\langle V_\infty\rangle)^2}{2kT}\right]V_\infty^{\,2}\,dV_\infty\times$$

$$\int_0^\infty \exp\left[\frac{-mV_\infty\langle V_\infty\rangle\delta^2}{2kT}\right]d\delta$$

Here we have extended the limits of integration for δ to $+\infty$ since $mV_\infty\langle B_\infty\rangle/2kT \gg 1$ and the exponential will cut off the integral. The δ integral can then be evaluated exactly. Integration over V_∞ is straightforward. The result is

$$n_{\mathrm{He}}(r,o) = n_{\mathrm{He}}(\infty)\left(\frac{\pi GMm}{rkT}\right)^{1/2}\exp\left[\frac{-\pi r_e^2 P(r_e)}{(2GMr)^{1/2}}\right]$$

Off-axis values of $n_{\mathrm{He}}(r,\delta)$ were constructed using the parabolic-interpolation formula

$$n_{\mathrm{He}}(r,\delta) = n_{\mathrm{He}}(r,o)(1 - D\delta^2)$$

where D is determined by the imposed constraint

$$n_{\mathrm{He}}(r,o)(1 - D\delta_c^{\,2}) = \frac{1}{\delta_c}n_{\mathrm{He}}(\infty)\left(\frac{2b}{r}\right)^{1/2}\times \exp\left[\frac{-\pi r_e^2 P(r_e)}{(2GMr)^{1/2}}\right]$$

at some angle δ_c. This yields

$$\delta_c = \frac{3}{2}\left(\frac{\pi m\langle V_\infty\rangle^2}{2kT}\right)^{-1/2}$$

and

$$D = \frac{2\pi m\langle V_\infty\rangle^2}{27kT}$$

The neutral He-normalized number density distribution is plotted in figure 3 as a function of ecliptic azimuth ϕ for $\langle V_\infty\rangle$ = 20 km/sec, T = 100° K, and r = 0.5 AU. The upper curve refers to direct orbits (characterized by impact parameter p_1), and the lower curve refers to indirect orbits (characterized by impact parameter p_2). The He density plotted in the neighborhood of ϕ = 270° is the sum of contributions from both direct and indirect orbits. Two important characteristics of the curves should be noted. First, in the forward hemisphere direct orbit densities dominate indirect orbit densities due to the much longer angular distance traveled by the latter. Second, there is a marked anisotropy (here 67:1) of number density in backward and forward directions resulting from an enhanced tail with FWHM = 3.1° for T = 100° K.

We now specify the ion position in the usual ecliptic polar coordinates r, θ, ϕ where r is the radial distance from the sun, θ is the polar angle with respect to the north ecliptic, and ϕ is the azimuthal angle with respect to the x axis. We further define χ as the angle between **r** and the magnetic field **B**. Then the Archimedean spiral magnetic field is given by

$$\left.\begin{aligned} B_r &= B_a\left(\frac{a}{r}\right)^2 \\ B_\theta &= 0 \\ B_\phi &= -B_a\left(\frac{a}{r}\right)^2\tan\chi \\ B &= B_a\left(\frac{a}{r}\right)^2\Big/\cos\chi \end{aligned}\right\} \qquad (2)$$

where $\cos\chi = [1 + (r\omega\sin\theta/V_{SW})^2]^{-1/2}$, the angular speed of the sun $\omega = 2.9\times10^{-6}$ rad/sec, B_a is the radial component of the magnetic field at some reference radius a, and V_{SW} is the radial solar wind velocity.

The equations governing the motion of a charged test particle in a slowly varying electric and magnetic field in the guiding center approximation were developed by *Northrop* [1963]. The motion can be separated into three components: (1) the superposition V_D of various drift velocities perpendicular to the magnetic field, (2) a circulating velocity $V_\perp$ about the magnetic field, (3) a velocity $V_\parallel$ parallel to the magnetic field. We now treat each of these components in turn specializing to the

above radially convected spiral magnetic field pattern.

The only perpendicular drift velocity of consequence is that due to the appearance of an electric field in the frame of reference at rest with respect to the sun. Here $V_D = V_{sw} \sin \chi$ with direction perpendicular to **B** but confined to the cone specified by θ = constant.

The component of motion circulating about **B** is determined in the adiabatic limit (which fits our problem) by the conservation of the magnetic moment μ, given by

$$\mu = \frac{mV_\perp^2}{2B} \tag{3}$$

The equation governing the motion parallel to the field direction given by *Northrup* [1963] is

$$\frac{mdV_\parallel}{dt} = mg_\parallel + qE_\parallel - \mu \frac{\partial B}{\partial s} + m\mathbf{V}_D \cdot \left[\frac{\partial \mathbf{e}_\parallel}{\partial t} + V_\parallel \frac{\partial \mathbf{e}_\parallel}{\partial s} + (\mathbf{V}_D \cdot \mathbf{V})\mathbf{e}_\parallel\right] \tag{4}$$

where m is the mass of the particle, the magnetic field direction is specified by the unit vector $\mathbf{e}_\parallel$, $g_\parallel$ is the component of the sun's gravitational acceleration along $\mathbf{e}_\parallel$, q is the particle charge, $E_\parallel$ is the component of electric field parallel to $\mathbf{e}_\parallel$, and s is arc length along $\mathbf{e}_\parallel$. In our problem $E_\parallel = 0$ and $\partial \mathbf{e}_\parallel / \partial t = 0$. Setting $\partial/\partial s = \mathbf{e}_\parallel \cdot \nabla$ in equation (4) and carrying through the algebra, we obtain

$$\frac{dV_\parallel}{dt} = \frac{\mu}{m}\frac{B\cos\chi}{r}(1+\cos^2\chi) - \frac{GM\cos\chi}{r^2} + \frac{V_{sw}\sin^2\chi}{r}[V_{sw}\cos^3\chi - V_\parallel(1+\cos^2\chi)] \tag{5}$$

The total noncirculating velocity is then given by

$$\mathbf{V} = V_\parallel \mathbf{e}_\parallel + \mathbf{V}_D$$

yielding

$$\frac{dr}{dt} = V_\parallel \cos\chi + V_{sw}\sin^2\chi \tag{6}$$

Combining equations (5) and (6) to eliminate the time, we obtain (after some algebra) an equation for $V_\parallel$ in terms of r alone:

$$d\left(\frac{V_\parallel^2}{2} + V_\parallel \frac{V_{sw}\sin^2\chi}{\cos\chi}\right) = dr\left[\frac{\mu}{m}\frac{B(r)}{r}(1+\cos^2\chi) - \frac{GM}{r^2} + (V_{sw}^2)\frac{\sin^2\chi\cos^2\chi}{r}\right] \tag{7}$$

Equation (5) can be integrated to yield

$$V_r = (V_\parallel \cos\chi + V_{sw}\sin^2\chi) = \pm \frac{V_{sw} f(\zeta)}{(1+\zeta^2)^{1/2}} - \tag{8}$$

$$V_\phi = (-V_\parallel \sin\chi + V_{sw}\sin\chi\cos\chi) = \frac{\zeta V_{sw}}{(1+\zeta^2)^{1/2}}\left[(1+\zeta^2)^{1/2} \mp f(\zeta)\right] \tag{9}$$

where

$$f(\zeta) = \left\{(\zeta^2 - \zeta_0^2) - \left(\frac{V_{\perp 0}}{V_{sw}}\right)^2\left[\frac{(1+\zeta^2)^{1/2}\zeta_0^2}{(1+\zeta_0^2)^{1/2}\zeta^2} - 1\right] + \left(\frac{2GM\omega\sin\theta}{V_{sw}^3}\right)\left(\frac{1}{\zeta} - \frac{1}{\zeta_0}\right) + \left[\frac{V_{\parallel 0}}{V_{sw}} + \frac{\zeta_0^2}{(1+\zeta_0^2)^{1/2}}\right]^2\right\}^{1/2} \tag{10}$$

Here $\zeta = \omega r \sin\theta / V_{sw}$ is a dimensionless radial distance, and all quantities appearing with a subscript zero refer to the initial conditions. The equation for the trajectory can be written in dimensionless form as

$$\frac{d\zeta}{d\phi} = \frac{\zeta \sin\theta\, V_r}{V_\phi} = \pm \frac{\sin\theta\, f(\zeta)}{[(1+\zeta^2)^{1/2} \mp f(\zeta)]} \tag{11}$$

where the minus and plus signs refer to motion in, toward or away from the sun, respectively.

To complete the problem the initial velocity conditions at the point of injection need be specified. We

consider first the trajectories resulting from a zero initial velocity and then proceed to the interstellar wind problem.

Zero-Velocity Initial Conditions

Here $V_{\|0} = 0$ and $V_{\perp 0} = V_D = V_{sw} \sin \chi_0$ since the orbits are initially cycloidal. Equation (11) was solved on the University of Wisconsin's Univac 1108 computer with a "Math-Pack" subroutine utilizing Hamming's method of solving ordinary first-order differential equations. The initial noncirculating velocity is perpendicular to **B** but away from the sun. Since B decreases as r increases, the conservation of the magnetic moment converts part of the circulating velocity into the parallel component. Specializing to the problem of injection into the unperturbed solar wind at Venus, the azimuthal angle as a function of radius characterizing the trajectory is plotted in figure 5. Components of the velocity as a function of r are plotted in figure 6. Again, $V_{sw} = 400$ km/sec. Since both the spiral field pattern and the initial injection conditions are azimuthally symmetric about the sun, there is no focusing of the particle beam in the ecliptic. Thus it's observed angular diameter should remain constant. Any deviation would then be due to interaction with magnetic irregularities convected by the wind.

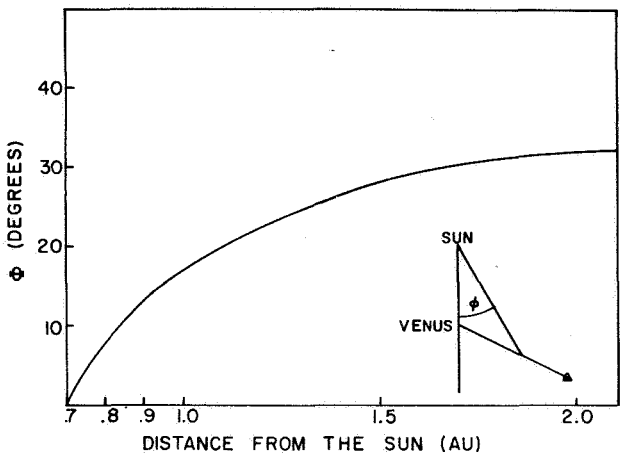

Figure 5 *Azimuthal position of a charged particle relative to the azimuthal position of injection into the solar wind at Venus.*

Interstellar Infall Initial Conditions

The neutral particle velocity at the point of ionization is determined by conservation of energy and angular momentum. For the indirect orbits $V_r = V_\infty[1 + 2b/r_O - (p_2/r_O)^2]^{1/2}$ and $V_\gamma = -V_\infty p_2/r_O$, where $b = GM/V_\infty^2$. For the direct orbits

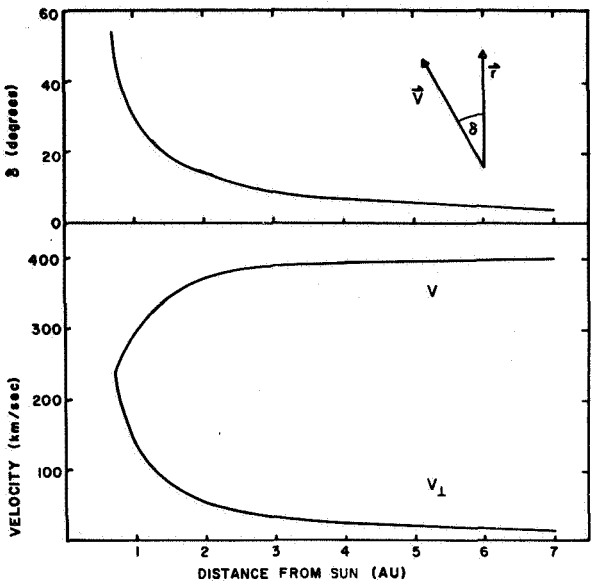

Figure 6 *Components of the velocity of a charged particle injected into the solar wind at Venus as a function of heliocentric distance.*

$V_r = \pm V_\infty[1 + 2b/r - (p_1/r)^2]^{1/2}$ where the $\pm$ refers to $\gamma \gtrless \gamma_{\min} = \tan^{-1}(-p_1/b)$ and $V_\gamma = V_\infty p_1/r_O$. The initial neutral velocity is $\mathbf{V}_N = V_r \mathbf{e}_r + V_\gamma \mathbf{e}_\gamma$ yielding $(V_{\|})_\infty = \mathbf{V}_N \cdot \mathbf{e}_{\|}$ and $(V_\perp)_\infty = \mathbf{V}_N - \mathbf{V}_N \cdot \mathbf{e}_{\|} - \mathbf{V}_D$. The effect of the asymmetry of these initial conditions with respect to azimuthal injection angle ϕ_0 on the subsequent trajectories is greater as r_0 decreases. This asymmetry is illustrated in figures 7 and 8 for injection from direct and indirect neutral orbits, respectively, at $r_0 = 0.15$ AU with V_∞ and r_0 in the ecliptic. The effect is most noticeable for the direct orbits characterized by $90° \leqslant \phi_0 \leqslant 270°$. As ϕ_0 increases from 90°, the magnetic moment decreases due to a cancellation effect reducing the magnetic mirror repulsion of the diverging field lines. Consequently, there is a region of impact angles around $\phi_0 = 180°$ for which ionized He atoms have access to the photosphere. This assumes a noise-free Archimedean spiral model extending all the way in to the photosphere which is not the case in reality. Proceeding further around in azimuthal angle, V_r decreases to zero as well, yielding trajectories that circulate about the sun through large angles before making their way out to large r. One such trajectory not plotted in figure 7 circled about the sun three times before reaching large r. Of course, such an orbit is unphysical due to interaction with magnetic irregularities but it illustrates the azimuthal focusing characteristics of the problem. The indirect orbits are illustrated in figure 8. These are much more regular but still demonstrate a degree of azimuthal

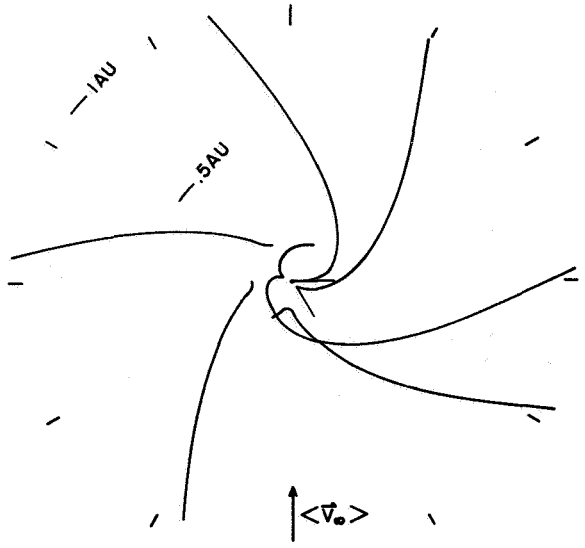

Figure 7 He^+ *orbits in an ideal spiral magnetic field following injection from direct neutral helium orbits:* $\langle V_\infty \rangle = 20$ *km/sec,* $\Theta = 90°$, $V_{SW} = 400$ *km/sec, and* $r_O = 0.15$ *AU.*

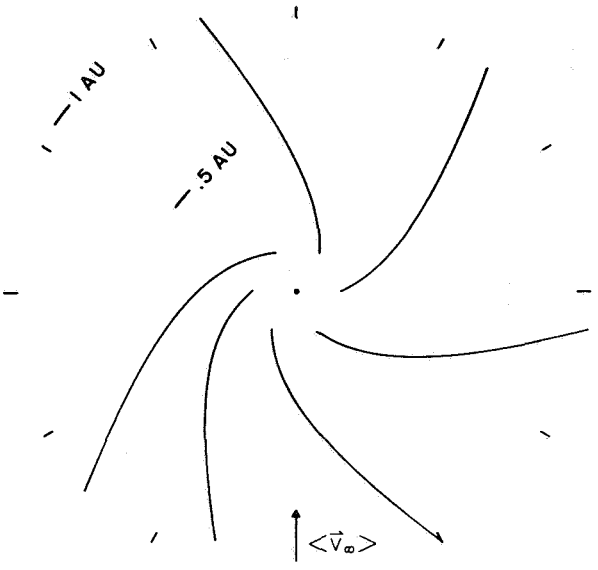

Figure 8 He^+ *orbits in an ideal spiral magnetic field following injection from indirect neutral helium orbits:* $\langle V_\infty \rangle = 20$ *km/sec,* $\Theta = 90°$, $V_{SW} = 400$ *km/sec, and* $r_O = 0.15$ *AU.*

focusing. The effects of the asymmetric initial conditions on the trajectories become less pronounced as the injection radius increases since the infall velocity becomes small compared to the drift velocity $V_D = V_{SW} \sin \chi$.

We are interested in calculating the He^+ velocity distribution function, which would be measured by a spacecraft observing at 1 AU in the ecliptic. Toward this end we need to know the locus of all source points for particle trajectories intersecting a given angular sector at 1 AU. This was accomplished numerically for 20° wide angular sectors centered on $\phi = 0°, 90°, 180°$, and 270°, for $\langle V_\infty \rangle = 10$, 20, and 40 km/sec, and for angles of incidence Θ with respect to the north ecliptic of 0°, 45°, and 90°. All orbits penetrating to r_O less than 0.05AU were excluded from consideration. Typical configurations are illustrated for direct and indirect orbits in figures 9 and 10 for $\langle V_\infty \rangle = 20$ km/sec and $\Theta = 45°$. As

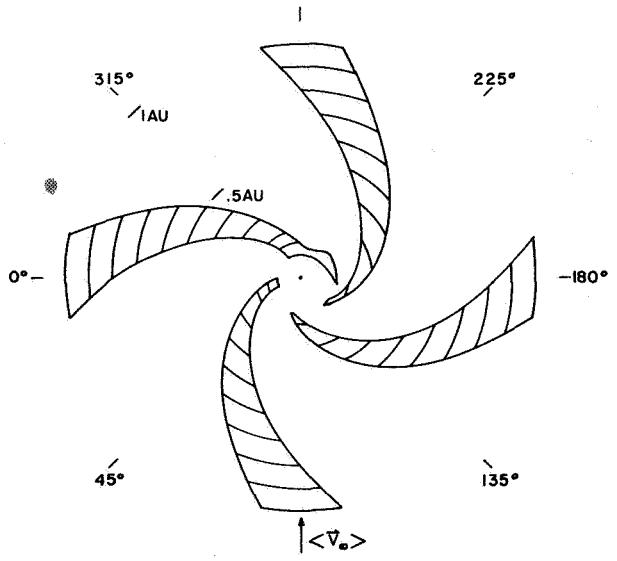

Figure 9 *Locus of source points of* He^+ *for detection at 1 AU following injection from direct neutral helium orbits:* $\langle V_\infty \rangle = 20$ *km/sec,* $\Theta = 45°$, $V_{SW} = 400$ *km/sec.*

can be seen, the focusing effect of the interplanetary fields becomes more prominent at small injection radii. For example, the locus of points intersecting the $\phi = 0°$ sector from $r_O = 0.15$ AU splits into two angular sectors at 0.15 AU due to the partial cancellation of the magnetic moment coupled with the changing sign (from minus to plus as ϕ_O increases past the angle of perihelion) of the initial radial velocity.

To construct the He^+ velocity distribution function we must sum separately the contributions enclosed within each sectored locus diagram for both direct and indirect orbits. Denoting direct neutral orbit initial conditions by $J = 1$ and indirect neutral orbits by $J = 2$, we

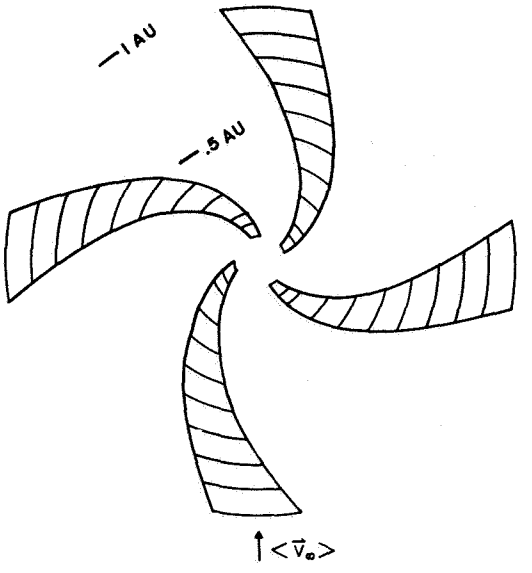

Figure 10 *Locus of source points of* He^+ *for detection at 1 AU following injection from indirect neutral helium orbits:* $\langle V_\infty \rangle = 20$ *km/sec,* $\Theta = 45°$, $V_{sw} = 400$ *km/sec.*

obtain from flux conservation

$$n^{(J)}_{He^+}(r_e,\phi_e) = \int_0^{r_e} \frac{dN^+}{dr_o}\, dr_o \qquad (12)$$

where

$$\frac{dN^+}{dr_o} = \frac{n^{(J)}_{He}(r_o,\phi_o)P(r_e)}{V_r^{(J)}(r_e,\phi_e;r_o,\phi_o)} \left(\frac{d\phi_o}{d\phi_e}\right) \qquad (13)$$

and $n^{(J)}_{He^+}(r_e,\phi_e)$ is the He^+ number density at the point (r_e,ϕ_e); $n^{(J)}_{He}(r_o,\phi_o)$ *is the neutral He number density at* the point (r_o,ϕ_o); $V_r^{(J)}(r_e,\phi_e;r_o,\phi_o)$ is the radial component of He^+ velocity at (r_e,ϕ_e) for those particles originating at (r_o,ϕ_o); and $d\phi_o/d\phi_e$ denotes the ratio of the azimuthal angular sector $d\phi_o$ at (r_o,ϕ_o) to the given sector $d\phi_e$ at (r_e,ϕ_e) into which $d\phi_o$ is mapped. The integral is evaluated along the locus sector.

The integrand of equation (12) is plotted as a function of r_o and ϕ_e in figures 11 through 14 for $\langle V_\infty \rangle = 10$, 20, and 40 km/sec and $\Theta = 45°$ and 0°. No plots for $\Theta = 90°$ are given due to the extreme anisotropy resulting from the presence of the dense, well-defined neutral-particle tail mentioned earlier. The definition of this tail depends strongly on the neutral gas temperature. For $T = 100°$ K its contribution to $n^{(J)}_{He^+}(r_e,\phi_e)$ depends critically on Θ since the FWHM of the tail is about 3°.

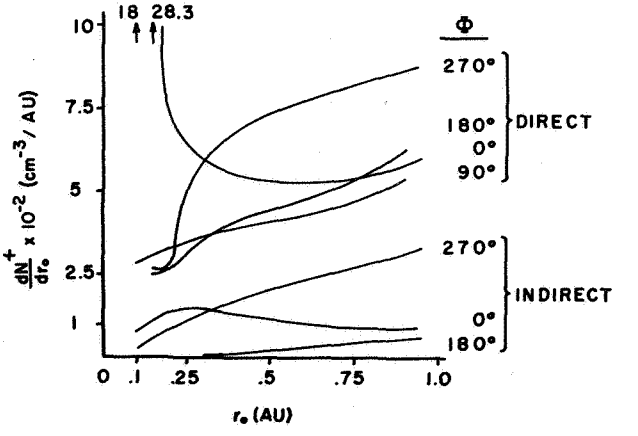

Figure 11 *Differential* He^+ *number density at 1 AU as a function of injection radius:* $\langle V_\infty \rangle = 10$ *km/sec,* $\Theta = 45°$; ϕ_e *denotes the azimuthal position of observation in the ecliptic.*

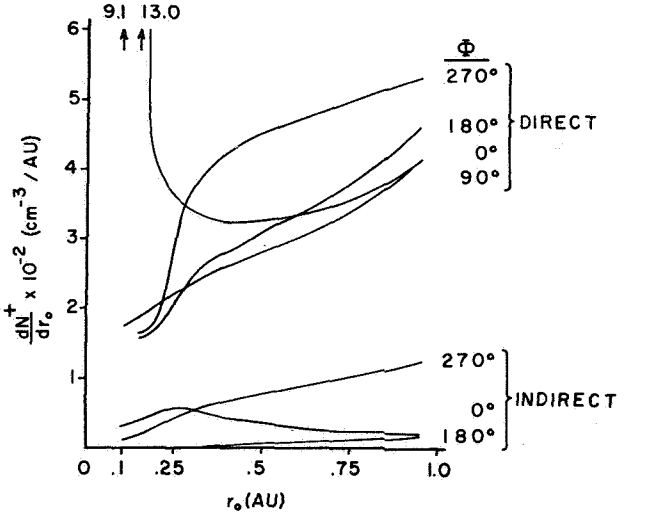

Figure 12 *Differential* He^+ *number density at 1 AU as a function of injection radius:* $\langle V_\infty \rangle = 20$ *km/sec,* $\Theta = 45°$; ϕ_e *denotes the azimuthal position of observation in the ecliptic.*

Furthermore, a crude (for 3° FWHM variation) 15° grid was used in our numerical analysis to calculate $n^{(J)}_{He^+}(r_e,\phi_e)$ and thus is not suited for calculation in this case.

For $\Theta = 90°$ and $T = 100°$ K, one might expect to observe anisotropies in $n^{(J)}_{He^+}(r_e,\phi_e)$ of the order of 50 (fig. 3).

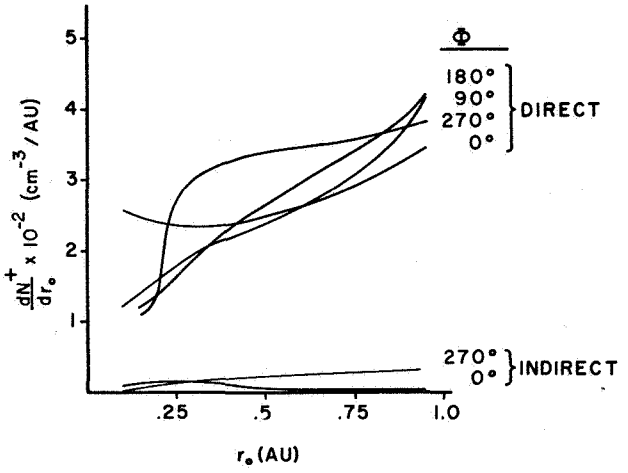

Figure 13 *Differential* He^+ *number density at 1 AU as a function of injection radius:* $\langle V_\infty \rangle = 40$ *km/sec,* $\Theta = 45°$; ϕ_e *denotes the azimuthal position of observation in the ecliptic.*

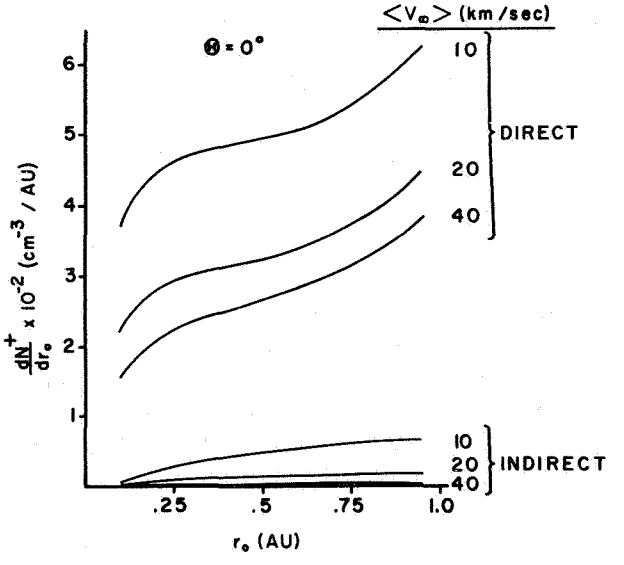

Figure 14 *Differential* He^+ *number density at 1 AU as a function of injection radius for* $\Theta = 0°$.

The He^+ number density at 1 AU integrated over velocity space and normalized to $n_{He}(\infty)$ is summarized in table 1 for $\Theta = 45°$ and 0° and $\langle V_\infty \rangle = 10$, 20, and 40 km/sec. It can be seen that $n^{(J)}_{He^+}(r_e,\phi_e)$ increases with decreasing $\langle V_\infty \rangle$ and that the anisotropy with respect to azimuthal phase ϕ_e at 1 AU increases with increasing Θ as well as decreasing $\langle V_\infty \rangle$. These effects primarily reflect the behavior of the neutral He number density in interplanetary space, but are also affected somewhat by the greater anisotropy of initial velocity conditions as Θ increases to 90°.

Table 1 *Integrated normalized* He^+ *number density* $n_{He^+}(r_e,\phi_e)/n_{He}(\infty)$ *at 1 AU*

$\Theta = 45°$				
$\langle V_\infty \rangle$ (km/sec)	$n_{He^+}(r_e,\phi_e)/n_{He}(\infty)$			
	$\phi_e = 90°$	$\phi_e = 180°$	$\phi_e = 270°$	$\phi_e = 360°$
10	3.8×10^{-2}	4.2×10^{-2}	7.9×10^{-2}	7.5×10^{-2}
20	2.7×10^{-2}	2.8×10^{-2}	4.4×10^{-2}	4.1×10^{-2}
40	2.4×10^{-2}	2.4×10^{-2}	3.0×10^{-2}	2.5×10^{-2}

$\Theta = 0°$	
$\langle V_\infty \rangle$ (km/sec)	$n_{He^+}(r_e)/n_{He}(\infty)$
10	5.0×10^{-2}
20	3.2×10^{-2}
40	2.5×10^{-2}

From equations (3), (8), and (9), we know the velocity of particles at 1 AU as a function of their injection position. Combining this information with dN^+/dr_0 from equation (13) we can construct the unperturbed velocity distribution function. Figure 15 shows a projection into the ecliptic of the position in velocity space occupied by ions with injection radii ranging between $r_0 = 0.15$ AU and 1.0 AU. The actual positions in velocity space are circles about **B** with diameters indicated in the figure. A spherical velocity contour of 20 km/sec about the solar wind velocity $V_{SW} = 400$ km/sec is sketched in for reference purposes. The minimum velocity angle with respect to the radial direction is 21° for the conditions $\langle V_\infty \rangle = 20$ km/sec, $\Theta = 45°$, and $\phi_e = 180°$. This minimum velocity angle for different sun-cloud configurations is tabulated in table 2. It is seen that this angle varies only slightly for markedly different incident conditions. The cone of occupation can change shape by at most 15 percent to 20 percent for the different incident conditions considered here. But since the distribution function is so diffuse to begin with, this is not a major effect.

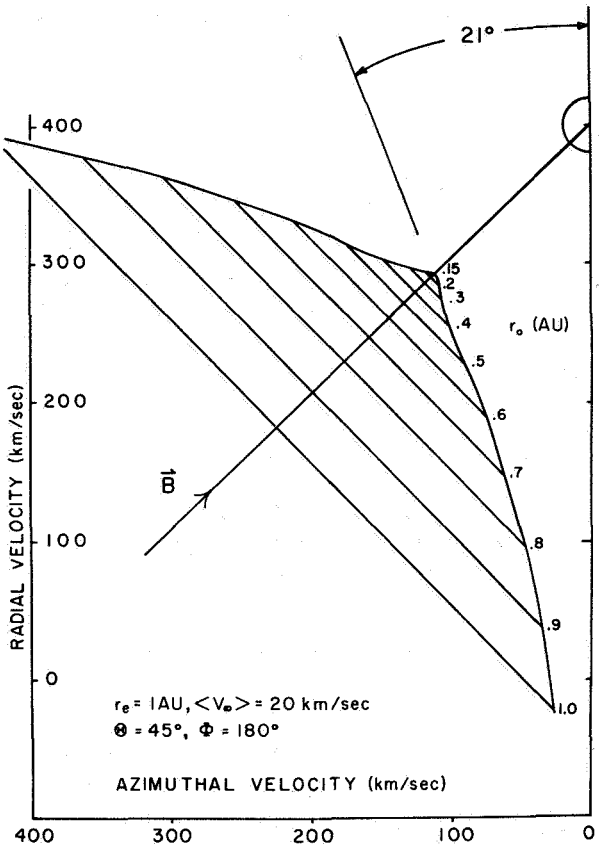

Figure 15 *Projection of the* He^+ *velocity distribution function into the ecliptic. Each line drawn perpendicular to* **B** *represents the diameter of a circle about* **B** *corresponding to* He^+ *ions injected into the solar wind at* $r = r_o$. *The circle about a radial velocity of 400 km/sec represents the projection of a sphere with 20 km/sec radius.*

Table 2 *Minimum velocity angle* β *of the* He^+ *velocity distribution function with respect to the radial direction*

$\Theta = 45°$				
$\langle V_\infty \rangle$ (km/sec)	β (deg)			
	$\phi_e = 90°$	$\phi_e = 180°$	$\phi_e = 270°$	$\phi_e = 360°$
10	20.0	21.0	22.1	19.9
20	19.8	20.8	22.1	19.7
40	19.4	20.7	22.0	19.3

$\Theta = 0°$	
$\langle V_\infty \rangle$ (km/sec)	β (deg)
10	21.2
20	21.1
40	20.9

DISCUSSION

We proceed now to the question of whether the model of cold interstellar He infalling into interplanetary space is consistent with the Vela 3 observations of He^+. The two relevant Vela 3 observational results are: (1) Most of the time, the ratio $n_{He^+}(r_e)/n_{He^{++}}(r_e)$ is less than 10^{-3}; and (2) on rare occasions, $n_{He^+}(r_e)/n_{He^{++}}(r_e)$ is observed to be $3\times10^{-3} \pm 50$ percent [*Bame et al.*, 1968].

Furthermore, we require that the model be consistent with recent observations of extraterrestrial diffuse Lyman α radiation observed with instruments on OGO 5 [*Thomas and Krassa*, 1971; *Bertaux and Blamont*, 1971]. To interpret these observations, *Thomas* [1971] considered two models of interstellar neutral hydrogen streaming relative to the sun. His first model required a cold (T = 100° K) streaming flow with $n_H(\infty) = 0.06\ cm^{-3}$; $\langle V_\infty \rangle \simeq 10$ km/sec oriented in the ecliptic, and an isotropic galactic Lyman α background of about 200 R. This was considered unlikely since current theories of the interstellar medium usually associate high temperatures ($T \simeq 10^4$ °K) with a hydrogen number density as low as $0.06\ cm^{-3}$. Furthermore, a calculation by *Adams* [1971] of the galactic Lyman α background radiation yielded an upper limit of 200 R without including the effects of Lyman α absorption due to interstellar dust grains. Thomas' second model requires a hot ($T \simeq 5\times10^3$ °K) flow with $n_H(\infty) \simeq 0.12\ cm^{-3}$, $\langle V_\infty \rangle \simeq 6$ km/sec oriented approximately in the ecliptic, and no galactic Lyman α background. (The upper limit of 2 R of 584Å radiation set by *Johnson et al.* [1971*b*] does not contradict the presence of neutral He consistent with the above models.)

The model of infalling interstellar gas considered in the present paper is valid for a finite gas temperature T at $r = \infty$ as long as $m\langle V_\infty \rangle^2 / 2\,kT >> 1$. For the cold model, $m\langle V_\infty \rangle^2 / 2kT = 243 >> 1$, and our results are applicable. But, for the hot model (V_∞ = 6 km/sec, T = 5000° K), $m\langle V_\infty \rangle^2 / 2kT = 1.72$ and our expressions for the neutral He number density in the antiapex region break down. In the following discussion we therefore concentrate on the cold interstellar gas model; the hot model will be discussed in a later paper.

As mentioned earlier, placement of $\langle V_\infty \rangle$ in the ecliptic results in large variations in $n_{He^+}(r_e, \phi_e)$. Figure 9 shows that enhanced fluxes are expected for

$270° \lesssim \phi_e \lesssim 360°$.

In the neighborhood of $\phi_e = 270°$ the major contribution comes from neutral He atoms ionized in the dense tail close to 1 AU (see figs. 3 and 9). These ions occupy the region at the base of the triangular cross section of the velocity distribution as indicated in figure 15. Since these ions travel a relatively small distance in the interplanetary field before reaching 1 AU, one does not expect much pitch angle scattering. Hence these ions would probably not contribute to a peak in an E/Q particle spectrum at $4(E/Q)_H$.

In the neighborhood of $\phi_e = 0°$, the major contribution comes from neutral He atoms ionized in the dense tail close to the sun. These ions normally occupy the region of velocity space at the apex of the triangular distribution which is closest to the solar wind velocity. In view of the evidence for enhanced noise in the solar wind near the sun, a high l value characterizing the initial pitch angle distribution of He^+ ions, and the long travel times to 1 AU, it is expected that a good fraction of these ions could be incorporated into the solar wind to contribute to a peak at $E/Q = 4(E/Q)_H$.

One might also expect a contribution to a peak at $4(E/Q)_H$ for azimuths in the range $100° \lesssim \phi_e \lesssim 240°$ (for radial ionization distances $0 < r_0 \lesssim 0.2$ AU). Here the magnetic moment is small so that He^+ ions penetrate deeply into the corona (see fig. 7). Such ions would be expected to be thermalized and therefore incorporated into the solar wind.

Last, a thermalized He^+ contribution is expected at $\phi_e = 270°$ due to neutral He in the tail ionized at $r_0 \lesssim 0.1$ AU. This He^+ number density is given by

$$n_{He^+}(r_e, 270°) = \int_0^{0.1\ AU} n_{He}(r_0, 270°)\frac{P(r_e)}{V_{sw}}\,dr_0$$

so that we obtain

$$\frac{n_{He^+}(r_e, 270°)}{n_{He^{++}}(r_e)} \sim 5\times10^{-4}$$

for $n_{He}(\infty) = 3\times10^{-3}$ cm^{-3}, $\langle V_\infty \rangle = 10$ km/sec, $T = 100°$K, $n_{He^{++}}(r_e) = 0.25$ cm^{-3}, $V_{sw} = 400$ km/sec and $P(r_e) = 6.8\times10^{-8}$ sec^{-1}. This ratio is not inconsistent with the Vela 3 result, but Vela 3 was at $\phi_e = 210°$ when the He^+ was observed.

One further comment with respect to the above calculations is in order. $P(r_e) = 6.8\times10^{-8}$ sec^{-1} was chosen on the basis of the solar EUV data of *Watanabe and Hinteregger* [1962]. A more recent measurement by *Hall and Hinteregger* [1970] revealed that the original measurements were systematically high. Use of the new data would decrease $P(r_e)$ and hence increase the neutral He density close to the sun. This would tend to make the He^+ density at 1 AU larger than the values calculated above. On the other hand, we did not include collisional ionization in calculating $P(r_e)$. This becomes important close to the sun which would tend to decrease $n_{He^+}(r_e, 270°)$.

Hundhausen et al. [1968] proposed, as an explanation of the Vela 3 measurements, that backstreaming hot neutral hydrogen atoms produced by charge exchange of solar wind protons with interstellar hydrogen at the heliosphere boundary could charge exchange with solar wind He^{++}, producing He^+. This mechanism requires the flux of incoming hot ($\langle V_\infty \rangle \sim 400$ km/sec) neutrals at 1 AU (which become ionized before leaving 1 AU out the reverse side) to be 1 percent of the solar wind flux of H^+. This fraction $F(r_e)$ can be estimated if we assume that all solar wind protons are converted to an isotropic flux of hot neutrals at the heliosphere boundary. Then if $f(H^+)$ is the flux density of solar wind protons at 1 AU, the total flux of fast H atoms backstreaming through any radius is $4\pi r_e^2 f$. The fast H atoms move along nearly rectilinear paths. Specifying the impact parameter of a backstreaming H atom by p and defining δ as previously, the probability α of an interaction within 1 AU is

$$\alpha = \exp\left[\frac{-r_e^2 P(r_e)(\pi - \delta)}{V_0 p}\right]\left\{1 - \exp\left[\frac{-r_e^2 P(r_e)(\pi + \delta)}{V_0 p}\right]\right\}$$

Then

$$F(r_e) = \int_0^{r_e}\left(\frac{\alpha}{4\pi R^2}\right)2\pi p\,dp$$

where R is the radius of the heliosphere. Integrating numerically, we obtain

$$F(r_e) = 0.088\left(\frac{r_e}{R}\right)^2$$

But R is expected to be at least 10 AU so that we obtain $F(r_e) \lesssim 10^{-3}$. This is an order of magnitude smaller than required by *Hundhausen et al.* [1968] to account for the Vela 3 measurement.

CONCLUSIONS

We conclude that although the possibility exists that $n_{He^+}(r_e,\phi_e)/n_{He^{++}}(r_e)$ in the solar wind is substantially higher than predicted from ionization equilibrium in a 10^6 °K expanding corona, it could be highly variable and depend strongly on ϕ_e, the azimuthal position of observation about the sun. We have shown that if the spiral magnetic field is noise free, the velocity distribution of He^+ at 1 AU is diffuse. Such a spectrum would not produce a peak at $4(E/Q)_H$ in an E/Q spectrum. If $\langle V_\infty \rangle$ is in the ecliptic, large variations in $n_{He^+}(r_e,\phi_e)$ with respect to ϕ_e are expected. Since solar wind magnetic irregularities are expected to be enhanced close to the sun, certain ϕ_e values will be more favorable than others for observing He^+ in a peak at $4(E/Q)_H$ in an E/Q spectrum. For example, azimuthal positions in the neighborhood of $100° \lesssim \phi_e < 240°$ corresponding to injection radii $0 < r_0 \lesssim 0.2$ AU receive contributions due to a cancellation of the initial magnetic moment, resulting in deeply penetrating He^+ orbits. This may result in effective thermalization. Another likely range of locations for observing thermalized He^+ ions is $270° \lesssim \phi_e \lesssim 360°$.

A value of $n_{He^+}(r_e)/n_{He^{++}}(r_e)$ in the solar wind of $\simeq 5 \times 10^{-4}$ can be predicted by the presence of a dense neutral tail due to interstellar infall. More He^+ is available from the interstellar infall, but a calculation of its relative magnitude appearing in a spectral peak requires a knowledge of the radial dependence of the power density spectrum of magnetic irregularities in the solar wind at times just preceding the observation.

It is interesting to note that the Vela 3 spectra with the anomalous peak attributed to He^+ were obtained on October 8. October 8 corresponds to $\phi_e = 210°$ for the earth. This is in the neighborhood where magnetic moment cancellation is expected to produce deep radial penetration and hence thermalization. Of course, deep penetration could also result in a second ionization yielding He^{++}. We feel that one should not place too much emphasis on a comparison of a single measurement with the ideas presented above.

ACKNOWLEDGMENTS

We are grateful for helpful conversations with A. Barnes and E. Roelof concerning pitch angle scattering and thermalization of charged particles in the solar wind. This work was supported under NASA Research Grants NGL 50-002-044 and NGR 50-002-162.

REFERENCES

Adams, T. F.: On Lyman-Alpha Emission From the Galaxy. *Astron. Astrophys.*, Vol. 12, 1971, p. 200.

Bame, S. J.; Asbridge, J. R.; Hundhausen, A. J.; and Montgomery, M. D.: Solar Wind Ions: $^{56}Fe^{+8}$ to $^{56}Fe^{+12}$, $^{28}Si^{+7}$, $^{28}Si^{+8}$, $^{28}Si^{+9}$, and $^{16}O^{+6}$. *J. Geophys. Res.*, Vol. 75, 1970, p. 6360.

Bame, S. J.; Hundhausen, A. J.; Asbridge, J. R.; and Strong, I. B.: Solar Wind Ion Composition. *Phys. Rev. Letters*, Vol. 20, 1968, p. 393.

Barnes, A.: Theory of Generation of Bow-Shock-Associated Hydromagnetic Waves in the Upstream Interplanetary Medium. *Cosmic Electrodyn.*, Vol. 1, 1970, p. 90.

Bertaux, J. L.; and Blamont, J. E.: Evidence for a Source of an Extraterrestrial Hydrogen Lyman-Alpha Emission: the Interstellar Wind. *Astron. Astrophys.*, Vol. 11, 1971, p. 200.

Coleman, P. J., Jr.: Variation in the Interplanetary Magnetic Field: Mariner 2, 1. Observed Properties. *J. Geophys. Res.*, Vol. 71, 1966, p. 5509.

Coleman, P. J., Jr.; Smith, E. J.; Davis, L., Jr.; and Jones, D. E.: The Radial Dependence of the Interplanetary Magnetic Field: 1.0–1.5 AU. *J. Geophys. Res.*, Vol. 74, 1969, p. 2826.

Fahr, H. J.: On the Influence of Neutral Interstellar Matter on the Upper Atmosphere. *Astrophys. Space Sci.*, Vol. 2, 1968, p. 474.

Hall, L. A.; and Hinteregger, H. E.: Solar Radiation in the Extreme Ultraviolet and Its Variations With Solar Rotation. *J. Geophys. Res.*, Vol. 75, 1970, p. 6959.

Hall, D. E.; and Sturrock, P. A.: Diffusion, Scattering, and Acceleration of Particles by Stochastic Electromagnetic Fields. *Phys. Fluids*, Vol. 10, 1967, p. 2620.

Holzer, T. E.; and Axford, W. I.: He^+ Ions in the Solar Wind. EOS, *Trans. Amer. Geophys. Union*, Vol. 51, 1970, p. 411.

Hundhausen, A. J.; Gilbert, G. E.; and Bame, S. J.: Ionization State of the Interplanetary Plasma. *J. Geophys. Res.*, Vol. 73, 1968, p. 5485.

Johnson, C. Y.; Young, J. M.; and Holmes, J. C.: Magnetoglow, a New Geophysical Resource. *Science*, Vol. 171, 1971*a*, p. 379.

Johnson, C. Y.; Young, J. M.; and Holmes, J. C.: To be published in *J. Geophys. Res.*, 1971*b*.

Northrup, T. G.: *The Adiabatic Motion of Charged Particles.* Interscience Pub., New York, 1963.

Patterson, T. N. L.; Johnson, F. S.; and Hanson, W. B.: The Distribution of Interplanetary Hydrogen. *Planet. Space Sci.*, Vol. 11, 1963, p. 767.

Sari, J. W.; and Ness, N. F.: Power Spectra of the Interplanetary Magnetic Field. *Solar Phys.*, Vol. 8, 1969, p. 155.

Siscoe, G. L.; Davis, L., Jr.; Coleman, P. J., Jr.; Smith, E. J.; and Jones, D. E.: Power Spectra and Discontinuities of the Interplanetary Magnetic Field: Mariner 4. *J. Geophys. Res.*, Vol. 73, 1968, p. 61.

Sturrock, P. A.: Stochastic Acceleration. *Phys. Rev.*, Vol. 141, 1966, p. 141.

Thomas, G. E.: Properties of Nearby Interstellar Hydrogen Deduced From Lyman-Alpha Sky Background Measurements. Preprint, 1971.

Thomas, G. E.; and Krassa, R. F.: OGO–5 Measurements of the Lyman-Alpha Sky Background. *Astron. Astrophys.*, Vol. 11, 1971, p. 218.

Tucker, W. H.; and Gould, R. J.: Radiation From a Low Density Plasma at 10^6-10^8 °K. *Astrophys. J.*, Vol. 144, 1966, p. 244.

Watanabe, K.; and Hinteregger, H. E.: Photoionization Rate in E and F Regions. *J. Geophys. Res.*, Vol. 67, 1962, p. 999.

Young, J. M.; Carruthers, G. R.; Holmes, J. C.; Johnson, C. Y.; and Patterson, N. P.: Detection of Lyman-Beta and Helium Resonance Radiation in the Night Sky. *Science*, Vol. 160, 1968, p. 990.